



Available online at www.sciencedirect.com

ScienceDirect

Procedia Structural Integrity 54 (2024) 34-43



International Conference on Structural Integrity 2023 (ICSI 2023)

Prediction of fatigue crack paths including crack-face friction for an inclined edge crack subjected to mixed mode loading

Sjoerd T. Hengeveld^{a,b,*}, Davide Leonetti^a, Bert Snijder^a, Johan Maljaars^{a,b}

^aStructural Engineering and Design, Eindhoven University of Technology, De Zaale 1, Eindhoven 5612 AZ, The Netherlands ^bReliable Structures, TNO, Molengraaffsingel 8, Delft 2629 JD, The Netherlands

Abstract

Accurately describing the fatigue crack growth rate and fatigue crack growth direction is crucial in determining the residual fatigue life of steel structures in general and for railway rails in particular. The crack growth rate and crack growth direction depend on the crack driving force. The stress intensity factor (SIF) is often considered as crack driving force and it depends on the applied load, the crack length and geometry. This paper concerns a numerical investigation on an inclined edge crack in a rail subjected to a moving patch load to evaluate its growth rate and direction including both normal and tangential stress components. A 2D finite element (FE) model is created including friction between the crack faces. The crack is incrementally extended in the predicted direction after each passage of the moving load. A parametric study is conducted to study the effect of the friction and traction coefficients. The results are compared in terms of predicted crack paths and SIF characteristics. It is shown that both friction and traction have a significant influence on the fatigue crack growth rate and path.

© 2023 The Authors. Published by Elsevier B.V. This is an open access article under the CC BY-NC-ND license (https://creativecommons.org/licenses/by-nc-nd/4.0) Peer-review under responsibility of the scientific committee of the ICSI 2023 organizers

Keywords: Crack growth direction; Mixed-mode fatigue crack growth; crack paths

1. Introduction

An accurate description of the crack growth rate and crack growth direction is crucial to accurately predict the remaining fatigue life of a steel structure. In some cases these structures are subjected to non-proportional multi-axial cyclic loading, for example in a wheel-rail system. The complex loading leads to rolling contact fatigue (RCF) see Zerbst et al. (2009). Cracks originating from the head of the rail are often decisive for maintenance. Increasing the prediction accuracy of the crack growth rate and crack growth direction reduces the usage of valuable maintenance resources. The crack growth rate and crack growth direction depend on the crack driving force. The stress intensity factor (SIF) is often considered as crack driving force in linear elastic fracture mechanics. The SIF is a function of the

^{*} Corresponding author E-mail address: s.t.hengeveld@tue.nl

applied load, the crack length and the geometry. Numerical methods such as finite element (FE) method are used to determine the SIFs for a complex geometry and complex loading conditions.

Several criteria are available to determine the fatigue crack growth direction. Most of them are developed for proportional loading, such as the maximum tangential stress (MTS) criteria, Erdogan and Sih (1963) and Sih (1974) the maximum shear stress criteria, Otsuka et al. (1975) and the maximum energy release rate criteria, Palaniswamy and Knauss (1972). For non-proportional loading, Hourlier and Pineau (1982) developed a method which is based on the maximum crack growth rate, supported by experimental results. The latter is used within the current research as the loading in RCF is non-proportional. Highsmith (2009) did an extensive research on crack growth direction theories.

Several studies determined the SIF evolution in the context of RCF for an inclined crack of a fixed length using the FE method. Dubourg and Lamacq (2002) investigated the effect of friction coefficient on the SIF evolution. Dallago et al. (2016) and Bogdański and Lewicki (2008) researched the effect of fluid entrapment on SIFs using 2D FE models. Naeimi et al. (2017), Afridi et al. (2022) and Nejad et al. (2016) investigated the SIF evolution in 3D.

The development of the extended finite element method (XFEM) allowed investigating growing cracks as the defect does not need to conform to the FE mesh. For example, Trollé et al. (2014) studied the crack propagation of an inclined edge crack using 2D XFEM with a non-linear material model, showing a significant influence of plasticity on the crack growth. Nezhad et al. (2022), developed a framework to predict the crack growth direction in a rail subjected to contact, bending and thermal loads. Leonetti and Vantadori (2022) estimated the SIFs of an inclined defect using weight functions thereby reducing the computational costs significantly compared to FE modelling. Generally, the previously mentioned research focussed on the stable crack growth regime, not including fracture. This paper concerns a numerical investigation on an inclined edge crack in a rail subjected to a moving patch load to evaluate its growth rate and direction including both normal and tangential stress components. The effect of different traction and friction coefficients on the predicted crack path is shown, taking into account both braking and accelerating traction forces. A framework is developed using conventional FE, assuming linear elastic material properties. First the framework is be described. Subsequently the results of the parametric analyses are given and discussed and finally conclusions and suggestions for future work are presented.

2. Fatigue crack growth and direction prediction model

The framework used to calculate the SIF and predict the crack path is shown in Figure 1. Four steps are defined. First, at step i=0, a FE model is created with Young's modulus E, Poisson ratio ν , and with an initial defect with length (a_0) , and predefined inclination angle (α_0) . Next the FE model is solved in multiple load steps, mimicking the translation of a moving load from left (location of center of load $x_c=x_b$) to right $(x_c=x_e)$, see Figure 2. This results in a mode I SIF (K_I) and mode II SIF (K_{II}) as function of the position of the load patch. Subsequently the fatigue crack growth rate (FCGR) and fatigue crack growth direction are determined. Finally the FE model is to be updated with the new crack increment, Δa . The individual steps are described in more detail in this section.

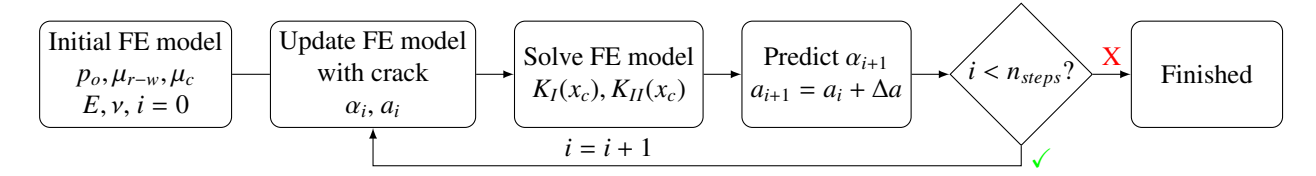


Fig. 1: Flowchart of the crack growth framework

2.1. Crack path calculations using the finite element method

A 2D plane strain FE model is formulated using Abaqus FEA. Geometrical non-linearity is considered. The model resembles a rectangular geometry with an inclined defect. The model is supported at the bottom edge, see Figure 2. The distribution of the vertical load follows a Hertzian contact stress. This distribution is applied at the top edge. The

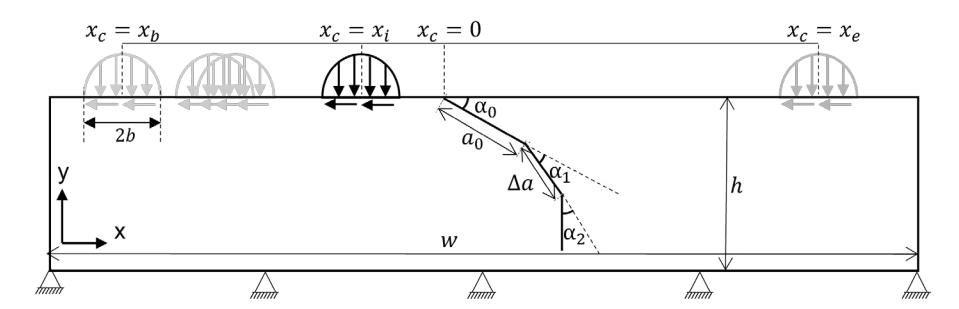


Fig. 2: Overview geometry

maximum stress $P_0 = 845$ MPa, which is an 2D approximation of a wheel load of 80 kN on a rail, assuming a 10 mm transversal contact width. Hertzian contact theory predicts a semi-elliptical normal stress distribution with a contact half width of b = 6.75 mm. Within one FE simulation, the load is translated from a begin position indicated with x_b and t_b to and end position indicated with x_e and t_e , see Figure 2. The stress distribution σ_n and shear stress distribution τ_{xy} K at every increment and location are defined by Equation 1.

$$\sigma_n(x, x_c) = \begin{cases} P_0 \sqrt{1 - \left(\frac{x - x_c}{b}\right)^2} & \text{if } |x - x_c| \le b\\ 0 & \text{otherwise} \end{cases}$$
 (1)

Assuming full sliding conditions, the tangential stress $\tau(x, x_c)$ is described by Equation 2.

$$\tau(x, x_c) = \mu_{r-w} \cdot \sigma_n(x, x_c) \tag{2}$$

in which μ_{r-w} is the constant traction coefficient. Braking results in $\mu_{r-w} > 0$ and acceleration is denoted with $\mu_{r-w} < 0$. Friction is assumed on the contact between the crack faces and is modelled using a Mohr-Coulomb friction model with friction coefficient μ_c . A structured FE mesh is used, with quadratic elements (type CPE8) using a full integration scheme. A refined mesh is used near the crack tip, see Figure 3. For a sharp crack the theoretical strain field at the crack tip in a FE model becomes singular. Using quadratic elements this singularity can be approximated by translating the midside nodes to the quarter point position close to the crack tip. Contact formulations using the penalty method including augmented Lagrange iterations are added between the crack faces to limit penetration.

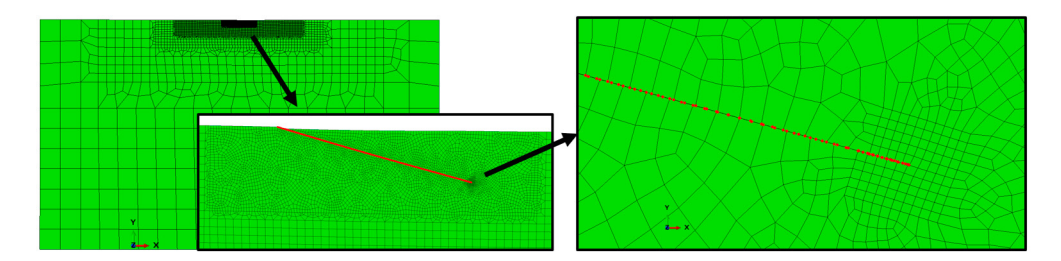


Fig. 3: Example of mesh refinement in FE model

The SIF in this study is computed using the virtual crack closure technique method. In VCCT the SIFs are calculated by assuming that the energy required to advance the crack with a small increment is the same as the energy required to close the crack for the same increment, see Rybicki and Kanninen (1977) and Krueger (2004). The equations derived by Raju (1987) are used within this study, see Equation 3 and Equation 4.

$$G_{1} = -\frac{1}{2\Delta a} F_{y'}^{c} \left(t_{11} \Delta U_{y'}^{m} + t_{12} \Delta U_{y'}^{n} \right) + F_{y'}^{j} \left(t_{21} \Delta U_{y'}^{m} + t_{22} \Delta U_{y'}^{n} \right)$$

$$G_{2} = -\frac{1}{2\Delta a} F_{x'}^{c} \left(t_{11} \Delta U_{x'}^{m} + t_{12} \Delta U_{x'}^{n} \right) + F_{x'}^{j} \left(t_{21} \Delta U_{x'}^{m} + t_{22} \Delta U_{x'}^{n} \right)$$
(3)

with:

$$\Delta U^{m} = U^{mt} - U^{mb}, \quad \Delta U^{n} = U^{nt} - U^{nb}$$

$$t_{11} = 6 - \frac{3\pi}{2}, \quad t_{12} = 6\pi - 20, \quad t_{21} = \frac{1}{2}, \quad t_{22} = 1$$
(4)

where G is the energy release rate, U are the nodal displacements and F are the nodal forces. The superscripts correspond to the nodes in Figure 4a. All values are evaluated in a rotated coordinate system x' and y' which is aligned with the crack in the current load increment (see Figure 4b). This alignment is based on the two elements in front of the crack tip. For every time step the energy release rates (G) are calculated, and subsequently these can be transformed to SIFs using Equation 5.

$$K_{I}(x_{c}) = \sqrt{G_{I}(x_{c})} E_{eff}$$

$$K_{II}(x_{c}) = \operatorname{sgn}(\Delta U_{x'}(x_{c})) \sqrt{G_{II}(x_{c})} E_{eff}$$
(5)

in which $E_{eff} = E$ for plane stress and $E_{eff} = \frac{E}{1-y^2}$ for plane strain.

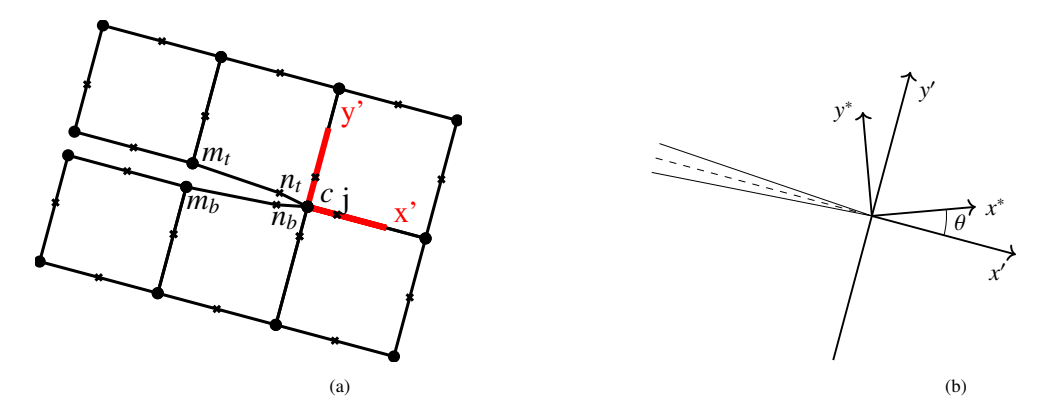


Fig. 4: (a) Schematic overview of mesh used in the quadratic VCCT algorithm (b) Coordinate system for determination of crack growth direction

The Hourlier and Pineau (1982) criterion assumes that the crack grows in the direction in which the SIFs of an infinitely small crack increment gives the highest FCGR. The SIFs of the (kinked) crack in the rotated coordinate system are calculated using the first order approximation of the stress field given by Cotterell and Rice (1980), see Equation 6.

$$\begin{bmatrix} K_I^*(\theta, x_c) \\ K_{II}^*(\theta, x_c) \end{bmatrix} = \frac{1}{4} \begin{bmatrix} 3\cos\frac{\theta}{2} + \cos\frac{3\theta}{2}, -3\left(\sin\frac{\theta}{2} + \sin\frac{3\theta}{2}\right) \\ \sin\frac{\theta}{2} + 3\sin\frac{3\theta}{2}, \cos\frac{\theta}{2} + 3\cos\frac{3\theta}{2} \end{bmatrix} \begin{bmatrix} K_I(x_c) \\ K_{II}(x_c) \end{bmatrix}$$
(6)

in which θ is the angle of the infinitely small (kinked) crack around the crack tip, see Figure 4b. To calculate the crack growth rate using these SIFs the equivalent stress range is calculated with:

$$\Delta K_I^* (\theta) = \max_{x_c} \left[\langle K_I^* (\theta, x_c) \rangle \right] - \min \left[\langle K_I^* (\theta, x_c) \rangle \right]$$

$$\Delta K_{II}^* (\theta) = \max_{x_c} \left[K_{II}^* (\theta, x_c) \right] - \min \left[K_{II}^* (\theta, x_c) \right]$$

$$\Delta K_{eq}^* (\theta) = \left(\Delta K_I^* (\theta)^2 + c_{II} \Delta K_{II}^* (\theta)^2 \right)^{0.5}$$
(7)

where $\langle \bullet \rangle$ are Macaulay brackets, $\langle \bullet \rangle = (\bullet + |\bullet|)/2$. The material constant $c_{II} = 0.772$ and is based on experimental fatigue crack growth data obtained for 900A (R260) rail steel, see Dubourg and Lamacq (2002). Finally the FCGR can be calculated using for example the equation developed by Paris et al. (1961), see Equation 8.

$$\frac{da}{dN}(\theta) = C\left(\Delta K_{eq}^*(\theta)\right)^m \tag{8}$$

where C, m are material properties. However, in these formulations for the equivalent SIF and the crack growth equation, sequence effects are not taken into account. Therefore, the angle which predicts the highest crack growth rate is equal to the angle of the highest equivalent SIF range, and the predicted crack growth angle is given by Equation 9.

$$\theta_{pred} = \underset{\theta}{\operatorname{argmax}} \, \Delta K_{eq}^* \left(\theta \right) \tag{9}$$

However the framework allows for more advanced crack growth laws. A comparison is made with the MTS criterium, Erdogan and Sih (1963). This criterion predicts the angle based on the SIF ranges, see Equation 10.

$$\Delta K_{I} = \max_{x_{c}} \left[K_{I}(x_{c}) \right] - \min_{x_{c}} \left[K_{I}(x_{c}) \right]$$

$$\Delta K_{II} = \max_{x_{c}} \left[K_{II}(x_{c}) \right] - \min_{x_{c}} \left[K_{II}(x_{c}) \right]$$
(10)

Subsequently, the angle is predicted by Equation 11

$$\theta_{pred}^{MTS} = -\operatorname{sgn}\left(\Delta K_{II}\right) \cos^{-1}\left(\frac{3\Delta K_{II}^2 + \sqrt{\Delta K_I^4 + 8\Delta K_I^2 \Delta K_{II}^2}}{\Delta K_I^2 + 9\Delta K_{II}^2}\right)$$
(11)

2.2. Update of finite element model

Following the previously determined direction, the FE model is updated taking a predefined step Δa , see Figure 1 An automated remeshing scheme is used to conform the mesh to the updated crack. Subsequently, the FE model can be solved for the updated geometry.

3. Results

3.1. Model verification

For verification of the model, the results from this study are compared with results from Trollé et al. (2014). In accordance with their study an initial crack length of a = 6 mm, angle $\alpha_o = 15$ deg, friction coefficient of $\mu_c = 0.1$ and traction coefficient of $\mu_{r-w} = 0.4$ are used. Figure 5 shows the results as a function of the normalized load position x/b, in which x/b = 0 means that the center of the contact patch load is above the crack mouth, see Figure 2. The solid lines in sub figures (a) and (b) are results obtained from Trollé et al. (2014). The other lines are the SIFs obtained within the current research for different element sizes. The elements around the crack tip have an element face length L_e of 8×10^{-2} mm, 2×10^{-2} mm or 5×10^{-3} mm. The elements near the crack faces are scaled accordingly, see Figure 6. Figure 5a shows the mode I results and Figure 5b shows the mode II results. No significant differences in results is seen using different element sizes, therefore in further analyses $L_e = 2 \times 10^{-2}$ mm is used. Differences at maximum K_{II} (max 10.0%) and maximum K_{II} (max 5.0%) can be seen between the results from Trollé et al. (2014) and the current implementation. These differences are attributed to the implementation of the crack, and SIF calculation method. In this study conventional FEM is used, and the SIF is calculated using the VCCT method. Trollé et al. (2014) use the XFEM method and calculates the SIFs using an energy approach.

Figure 5c shows the predicted crack path after approximately 0.7 mm crack growth for different crack increments Δa . Small oscillations in the predicted crack path can be seen. However, the trend of the three paths is similar. Therefore $\Delta a = 0.1$ mm is used in the remainder of this study. Based on these results, it is assumed that the current framework is able to predict the SIF distribution and crack path for a two-dimensional inclined edge crack, subjected to a moving patch load.

3.2. Influence of friction coefficient

Friction between the crack faces reduces the mode II SIF. However, determining the friction coefficient is non-trivial, since fluid, debris and other lubricants could influence the frictional behaviour. The uncertainty in the fric-

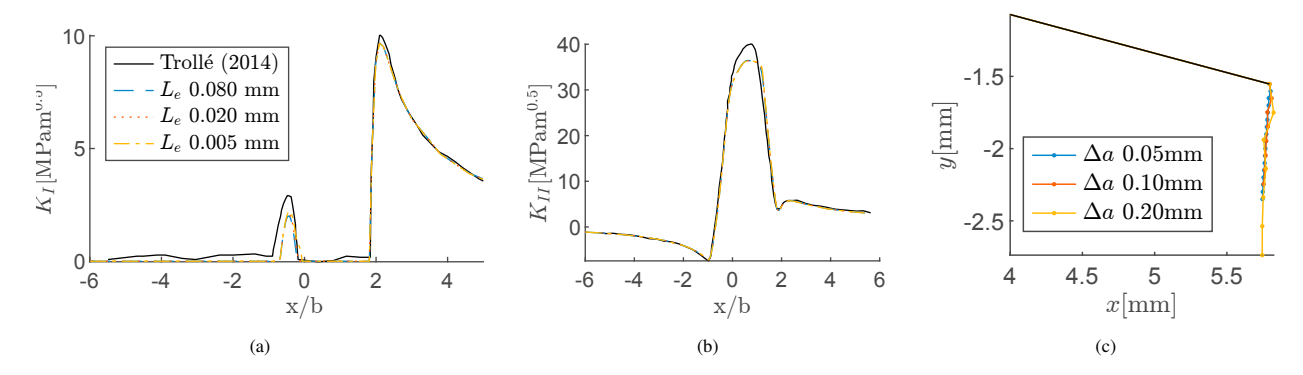


Fig. 5: SIFs as function of relative loading position; (a) mode I SIF, (b) mode II SIF, (c) Predicted crack paths for different crack increments Δa

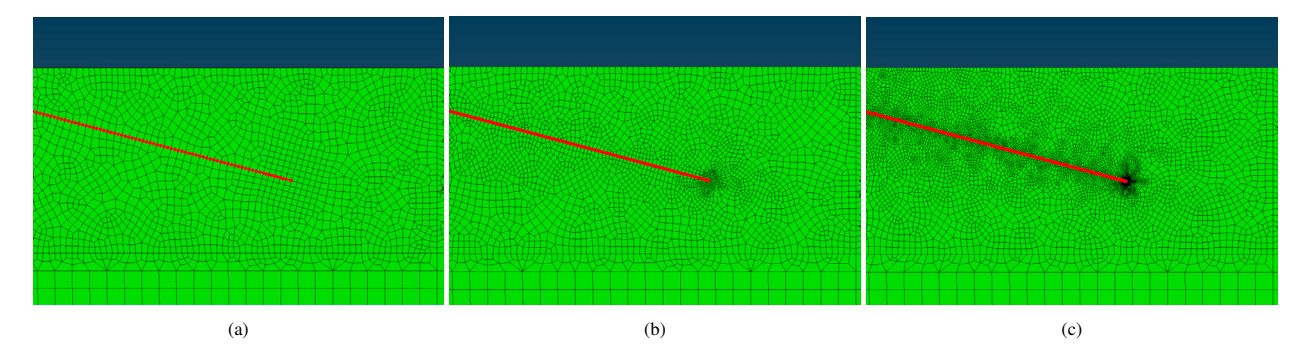


Fig. 6: Element meshes: (a) $L_e = 8 \times 10^{-2}$ mm, $L_e = 2 \times 10^{-2}$ mm, $L_e = 5 \times 10^{-3}$ mm

tional behaviour is included by changing the assumed friction coefficient in the Mohr-Coulomb friction model. This subsection shows the effect of various friction coefficients on the SIF evolution for an inclined edge crack.

All simulations are made with $a_o = 6$ mm and $\alpha = 15$ deg. Two different traction coefficients are used, namely, $\mu_{r-w} = 0.2$ and $\mu_{r-w} = 0.4$. Figure 7 shows the results in terms of SIF. The influence of μ_c on K_I appears to be limited. The crack opens when the load reaches the crack mouth, i.e x/b = 0. Due to the crack inclination angle, the crack opening is counteracted by the friction force, so an increase in friction coefficient reduces the max K_I . For $0 \le x/b < 2$, a large part of the load patch is above the crack, causing it to close, and therefore K_I is zero. For x/b > 2 the crack is fully open causing that there is no effect of the friction coefficient on K_I . The effect of the friction coefficient on K_{II} is reduced with increasing friction coefficient in the interval $0 \le x/b < 2$. For a high friction coefficient of $\mu_c = 0.5$, the location of maximum K_{II} shifts from $x/b \approx 0.6$, with the load above the crack mouth, to x/b > 2.0 with the load on the right side of the crack. Figure 7c shows the minimum (crosses) K_{II} and maximum (circles) K_{II} as a function of the friction coefficient. The dashed lines are results of the current research, the solid lines are results for the same geometry obtained by Dubourg and Lamacq (2002). The blue and red curves are results obtained with $\mu_{r-w} = 0.2$ and $\mu_{r-w} = 0.4$, respectively. The results are in good agreement with the results obtained in Dubourg and Lamacq (2002).

The minimum value of K_{II} , K_{II}^{min} is insensitive to μ_c , because it occurs when the crack is fully open ($K_I > 0$). On the other hand, the maximum K_{II} decreases significantly with increasing friction coefficient. Based on these results, it is shown that a good approximation of the friction coefficient is essential in determining the FCGR.

Figure 7d shows the predicted crack paths for several friction coefficients, using the previously defined framework, with a fixed crack increment of $\Delta a=0.1$ mm and $\mu_{r-w}=0.4$. A low friction coefficient results in a large K_{II} component, leading to a sharp angle. However the predicted path of the crack with $\mu_c=0.5$ is in between those of $\mu_c=0.1$ and $\mu_c=0.3$. This is due to the previously mentioned change of location of the maximum K_{II} , from $x/b\approx0$ for $\mu_c\leq0.3$ to $x/b\approx2.5$ for $\mu_c=0.5$, see Figure 7b. It should be noted that this predicted crack path is strongly dependent on the considered loads and boundary conditions. For future work it is recommended to expand the loads,

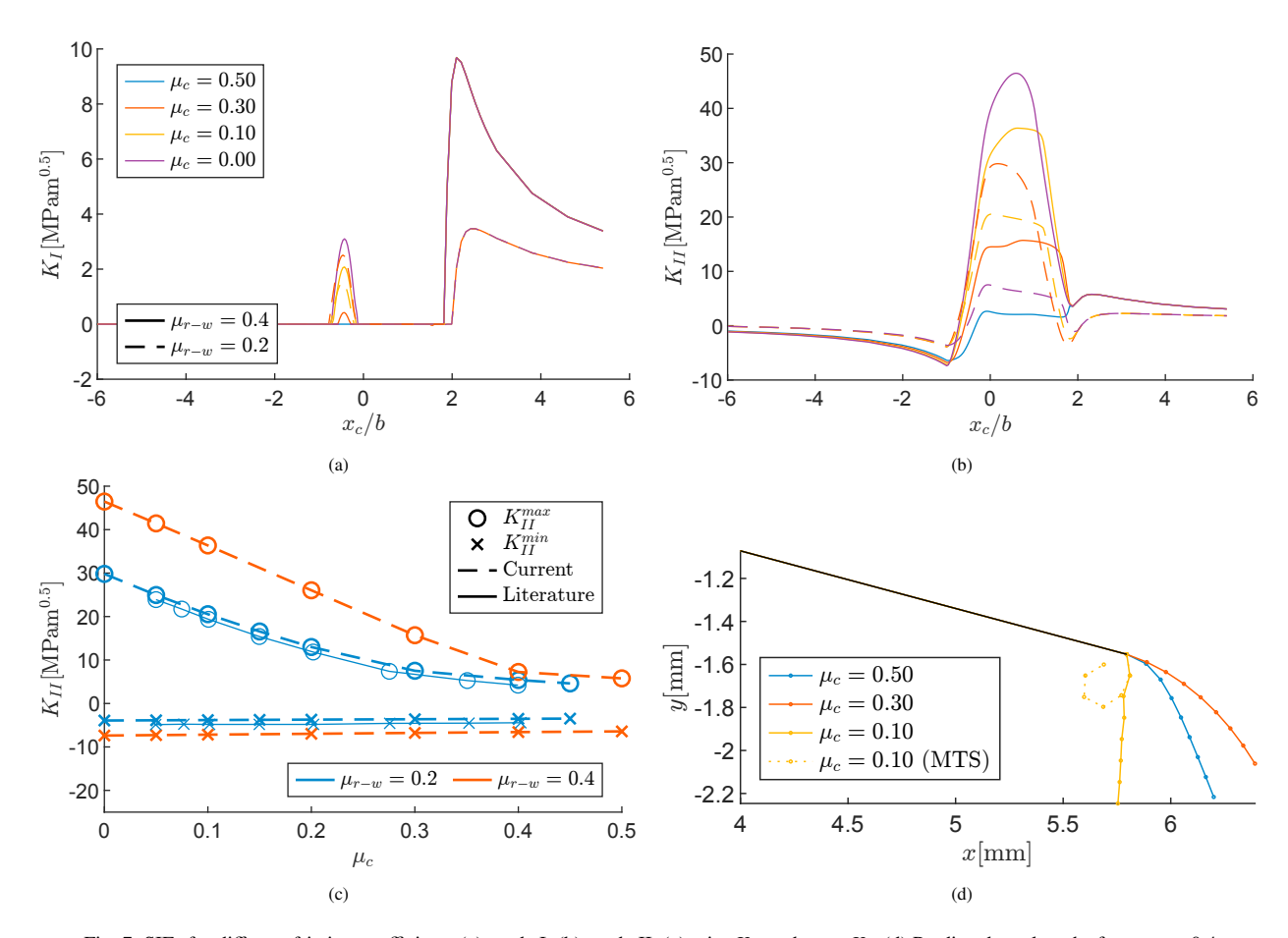


Fig. 7: SIFs for different friction coefficients (a) mode I, (b) mode II, (c) min. K_{II} and max. K_{II} (d) Predicted crack paths for $\mu_{w-r} = 0.4$

with for example bending and thermal loads. The dashed yellow line is the predicted crack path when using the MTS criterium. This criterium is originally developed for proportional loading and is therefore not applicable to the case of an inclined crack, as shown.

3.3. Influence of traction coefficient

In this section the influence of the traction coefficient is studied and the results are shown in Figure 8. Distinction is made between two friction coefficients $\mu_c = 0.1$ and $\mu_c = 0.5$. Figure 8a shows the evolution of K_I as a function of the load position. The different colors represent different traction coefficients. The dashed curves are the results for $\mu_c = 0.1$ and the solid curves are the results for $\mu_c = 0.5$. Figure 8c shows the minimum and maximum of K_I of the entire load path as a function of the traction coefficient. The crack is open at K_I^{max} , hence there is a limited influence of the crack face friction (corresponding to the results of Figure 7a). As expected, K_I^{max} is minimum when there is no traction force applied because the traction load opens the inclined crack when passing over the rail. A braking traction force $\mu_{r-w} > 0$ leads to a higher maximum K_I component than an accelerating traction load, with the same absolute traction coefficient.

In a similar way Figure 8b shows the results for K_{II} . Figure 8d shows the minimum (crosses) K_{II} , maximum K_{II} (circles) and maximum ΔK_{II} range (diamonds). From both figures a significant difference in SIF is seen between the low and the high friction coefficient: The latter gives a lower K_{II}^{max} , which is due to the increased load fraction transferred by friction, thereby shielding the crack tip. The minimum values are obtained when the traction coefficient is zero. In mode II both a positive as well as negative traction coefficient results in a significant increase in SIF range.

Figure 8e shows the predicted crack paths after approximately 1 mm crack growth with a fixed load step of $\Delta a = 0.1$ mm. Depending on the traction coefficients the crack does or does not to deviate from the initial direction. For $\mu_{r-w} = -0.4$ the crack starts to grow upward due to the high negative K_{II} value. In practice, spalling of part of the rail head is sometimes seen. This could indicate upwards crack growth, however, such a a sharp deviation upwards is probably not realistic. It is foreseen that adding additional loads, such as bending and thermal loads, will alter these crack paths.

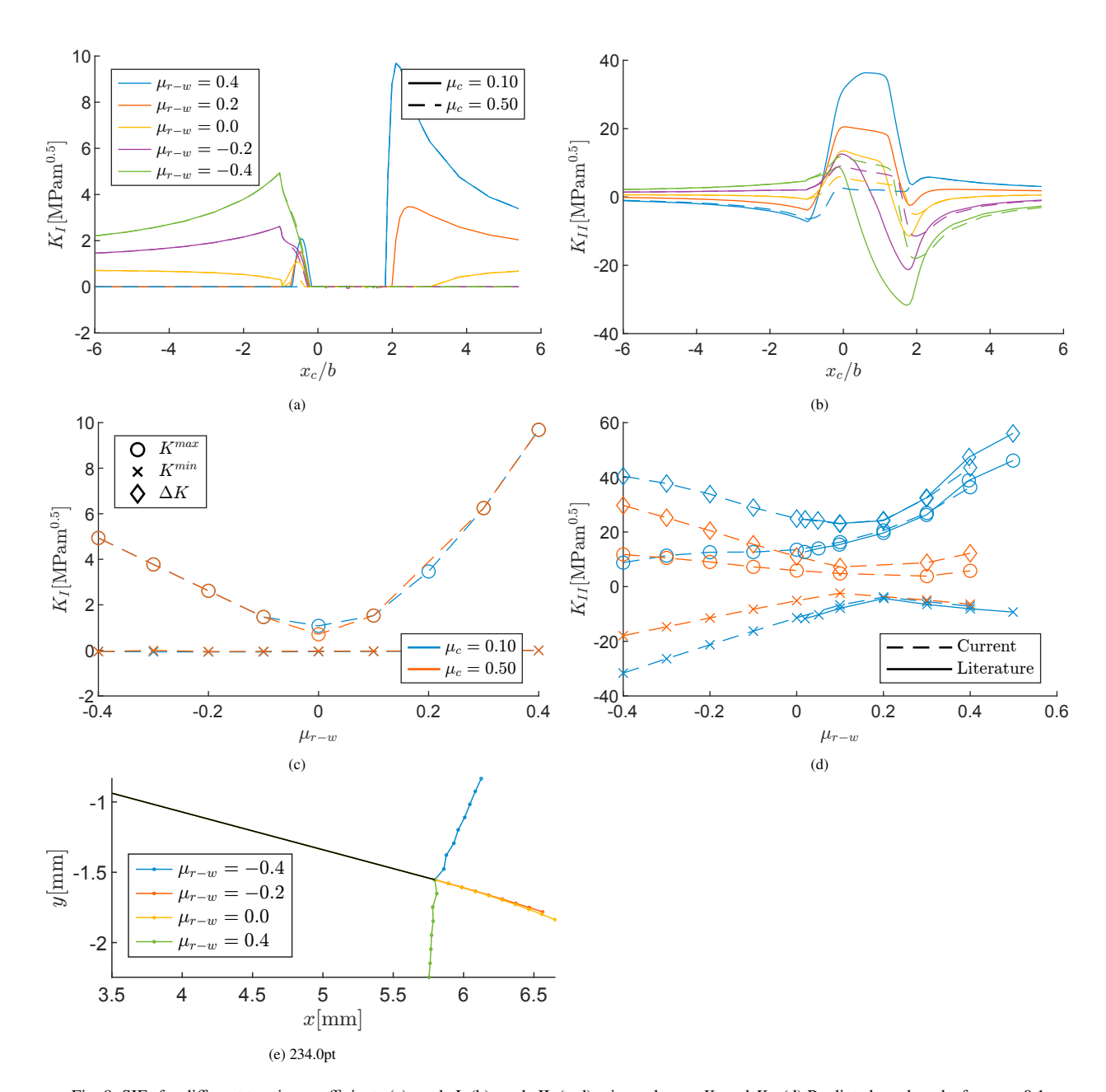


Fig. 8: SIFs for different traction coefficients (a) mode I, (b) mode II, (c-d) min. and max. K_I and K_{II} (d) Predicted crack paths for $\mu_c = 0.1$

4. Discussion

From the above shown results it is clear that both the friction and traction coefficient have a significant influence on the predicted crack path. The current predicted crack paths are a result of the applied loading conditions and boundary condition. Nezhad et al. (2022, 2023) investigated the influence of bending and thermal loads on the predicted crack growth. The crack path is predicted using the vector crack tip displacement technique, which is based on displacements at the crack tip. They concluded that the addition of bending and thermal load results in a more downward orientated crack path than for the case of pure contact loading. It is expected that a significant effect applies to the cases studied here. The residual stress field originating from manufacturing also influences the local stress state and should therefore also be included in a complete framework. The effect of other modelling assumptions, such as the idealization of the wheel-rail contact by a Hertzian contact distribution, should be verified with more complex (FE) models, possibly including the wheel. The used crack growth Equation 8 assumes that the fatigue crack growth rate (FCGR) can be estimated solely based on the equivalent SIF range. However, it is known that the FCGR of (rail)steel depends on the mean stress, see Kim and Kim (2002). Incorporating a mean stress corrected crack growth equation would give the opportunity to quantify the crack growth rate.

Additionally, Nezhad et al. (2022, 2023) showed an effect of the crack face friction on the predicted crack paths. This effect, appears to be smaller than predicted by the current study. However, a quantitative comparison is not possible due to a different crack geometry and crack prediction algorithm. Therefore, it is recommended to first validate the Hourlier-Pineau direction algorithm with relevant experimental data and to determine relevant friction coefficients.

The current study is limited to 2D, whereas defects in rails are complex 3D geometries. The above mentioned modelling assumptions imply that the current model is unable to give a quantitative fatigue life. However, the model shows the importance of traction and friction on predicted crack growth paths.

5. Conclusions and future work

This paper describes a framework to predict the crack growth direction for an inclined edge crack in a finite width plate subjected to a moving load patch following a Hertz contact stress distribution. The framework consists of a FE model with an incrementally updated crack. It is concluded that:

- A framework is developed which can be easily extended with additional loads including thermal loads and residual stresses.
- The assumed friction coefficient between the crack faces has a significant influence on the predicted crack paths as the mode II SIF is dominating the crack growth behaviour.
- An increase in traction coefficient leads to an increase in both K_I and K_{II} . A negative traction coefficient, hence accelerating of the wheel, leads to small increase in K_I compared to a free rolling wheel and a more significant increase in K_{II} .
- The predicted crack paths are highly dependent on the friction and traction coefficients. The applicability of the Hourlier Pineau criterium to predict the crack growth direction needs to be verified with experimental data. The MTS criterium predicts unrealistic crack paths for this application.
- Extension of the model in three dimensions allows for investigating more complex and realistic crack shapes.

6. Acknowledgement

This research was carried out under project number T20008 in the framework of the Research Program of the Materials innovation institute (M2i) (www.m2i.nl) supported by the Dutch government. ProRail is acknowledged for their contribution to this research.

References

- Afridi, A.H., Zhu, H., Camacho, E.T., Deng, G., Li, H., 2022. Numerical modeling of rolling contact fatigue cracks in the railhead. Engineering Failure Analysis, 106838doi:10.1016/j.engfailanal.2022.106838.
- Bogdański, S., Lewicki, P., 2008. 3D model of liquid entrapment mechanism for rolling contact fatigue cracks in rails. Wear 265, 1356–1362. doi:10.1016/j.wear.2008.03.014.
- Cotterell, B., Rice, J., 1980. Slightly curved or kinked cracks. International Journal of Fracture 16, 155–169. doi:10.1007/bf00012619.
- Dallago, M., Benedetti, M., Ancellotti, S., Fontanari, V., 2016. The role of lubricating fluid pressurization and entrapment on the path of inclined edge cracks originated under rolling–sliding contact fatigue: Numerical analyses vs. experimental evidences. International Journal of Fatigue 92, 517–530. doi:10.1016/j.ijfatigue.2016.02.014.
- Dubourg, M.C., Lamacq, V., 2002. A predictive rolling contact fatigue crack growth model: Onset of branching, direction, and growth—role of dry and lubricated conditions on crack patterns. Journal of Tribology 124, 680–688. doi:10.1115/1.1479698.
- Erdogan, F., Sih, G.C., 1963. On the crack extension in plates under plane loading and transverse shear. Journal of Basic Engineering 85, 519–525. doi:10.1115/1.3656897.
- Highsmith, S., 2009. Crack path determination for non-proportional mixed-mode fatigue. Ph.D. thesis. George W. Woodruff School of Mechanical Engineering.
- Hourlier, F., Pineau, A., 1982. Propagation of fatigue cracks under polymodal loading. Fatigue & Fracture of Engineering Materials and Structures 5, 287–302. doi:10.1111/j.1460-2695.1982.tb01237.x.
- Kim, J.K., Kim, C.S., 2002. Fatigue crack growth behavior of rail steel under mode I and mixed mode loadings. Materials Science and Engineering: A 338, 191–201. doi:10.1016/s0921-5093(02)00052-7.
- Krueger, R., 2004. Virtual crack closure technique: History, approach, and applications. Applied Mechanics Reviews 57, 109–143. doi:10.1115/
- Leonetti, D., Vantadori, S., 2022. On the growth of rolling contact fatigue cracks using weight functions. Procedia Structural Integrity 39, 9–19. doi:10.1016/j.prostr.2022.03.067.
- Naeimi, M., Li, Z., Dollevoet, R., 2017. Computation of stress intensity factors in an initiating rcf crack using a 3D modelling approach, in: Proceedings of the First International Conference on Rail Transportation:ICRT2017.
- Nejad, R.M., Farhangdoost, K., Shariati, M., 2016. Three-dimensional simulation of rolling contact fatigue crack growth in UIC60 rails. Tribology Transactions 59, 1059–1069. doi:10.1080/10402004.2015.1134738.
- Nezhad, M.S., Floros, D., Larsson, F., Kabo, E., Ekberg, A., 2022. Numerical predictions of crack growth direction in a railhead under contact, bending and thermal loads. Engineering Fracture Mechanics 261, 108218. doi:10.1016/j.engfracmech.2021.108218.
- Nezhad, M.S., Larsson, F., Kabo, E., Ekberg, A., 2023. Numerical prediction of railhead rolling contact fatigue crack growth. Wear 530-531, 205003. doi:10.1016/j.wear.2023.205003.
- Otsuka, A., Mori, K., Miyata, T., 1975. The condition of fatigue crack growth in mixed mode condition. Engineering Fracture Mechanics 7, 429–439. doi:10.1016/0013-7944(75)90043-0.
- Palaniswamy, K., Knauss, W.G., 1972. Propagation of a crack under general, in-plane tension. International Journal of Fracture Mechanics 8, 114–117. doi:10.1007/bf00185207.
- Paris, P., Gomez, M., Anderson, W., 1961. A rational theory of fatigue. The Trend of Engineering 13, 9 14. URL: https://www.scopus.com/inward/record.uri?eid=2-s2.0-85120384671&partnerID=40&md5=50c0794a38fa646afe002a0f8c79daf8. cited by: 1.
- Raju, I., 1987. Calculation of strain-energy release rates with higher order and singular finite elements. Engineering Fracture Mechanics 28, 251–274. doi:10.1016/0013-7944(87)90220-7.
- Rybicki, E., Kanninen, M., 1977. A finite element calculation of stress intensity factors by a modified crack closure integral. Engineering Fracture Mechanics 9, 931–938. doi:10.1016/0013-7944(77)90013-3.
- Sih, G.C., 1974. Strain-energy-density factor applied to mixed mode crack problems. International Journal of Fracture 10, 305–321. doi:10.1007/bf00035493.
- Trollé, B., Baietto, M.C., Gravouil, A., Mai, S., Prabel, B., 2014. 2D fatigue crack propagation in rails taking into account actual plastic stresses. Engineering Fracture Mechanics 123, 163–181. doi:10.1016/j.engfracmech.2014.03.020.
- Zerbst, U., Schodel, M., Heyder, R., 2009. Damage tolerance investigations on rails. Engineering Fracture Mechanics 76, 2637–2653. doi:10.1016/j.engfracmech.2008.04.001.